Cell Reports, Volume *40*

Supplemental information

Genetic impairment of succinate metabolism disrupts bioenergetic sensing in adrenal neuroendocrine cancer

Priyanka Gupta, Keehn Strange, Rahul Telange, Ailan Guo, Heather Hatch, Amin Sobh, Jonathan Elie, Angela M. Carter, John Totenhagen, Chunfeng Tan, Yogesh A. Sonawane, Jiri Neuzil, Amarnath Natarajan, Ashley J. Ovens, Jonathan S. Oakhill, Thorsten Wiederhold, Karel Pacak, Hans K. Ghayee, Laurent Meijer, Sushanth Reddy, and James A. Bibb

Supplemental Figures

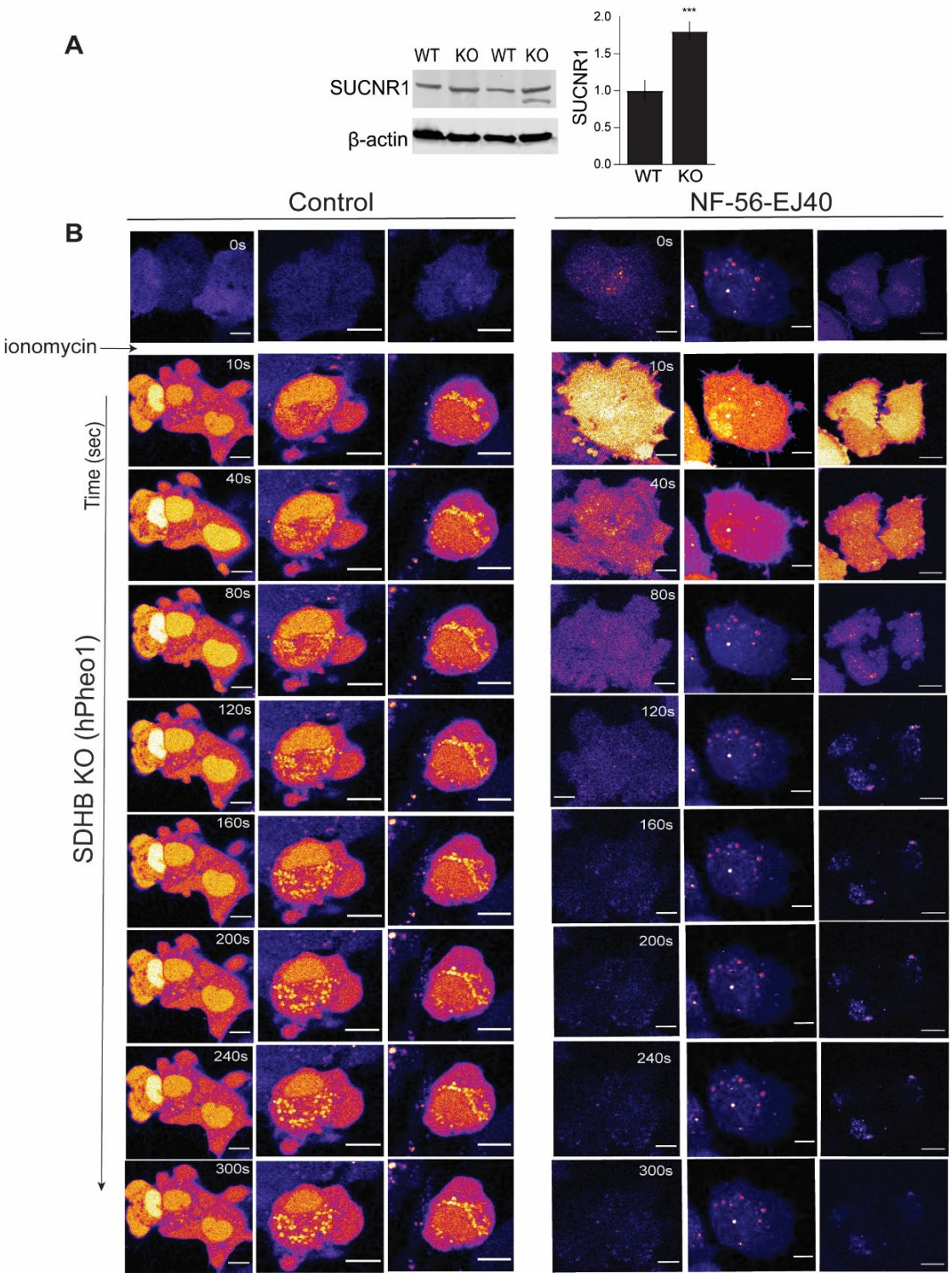

Figure S1. Loss of *SDHB* perturbs SUCNR1-mediated Ca^{2+} homeostasis (Related to Main Fig. 2). (A) Relative SUCNR1 expression in WT vs. *SDHB* KO cells. Values are means ± S.E.M., ***p < 0.001. (B) Supplemental confocal time lapse images showing $[Ca^{2+}]_i$ changes in control vs. NF-56-EJ40 treated cells as indicated in response to ionomycin (10 μM).

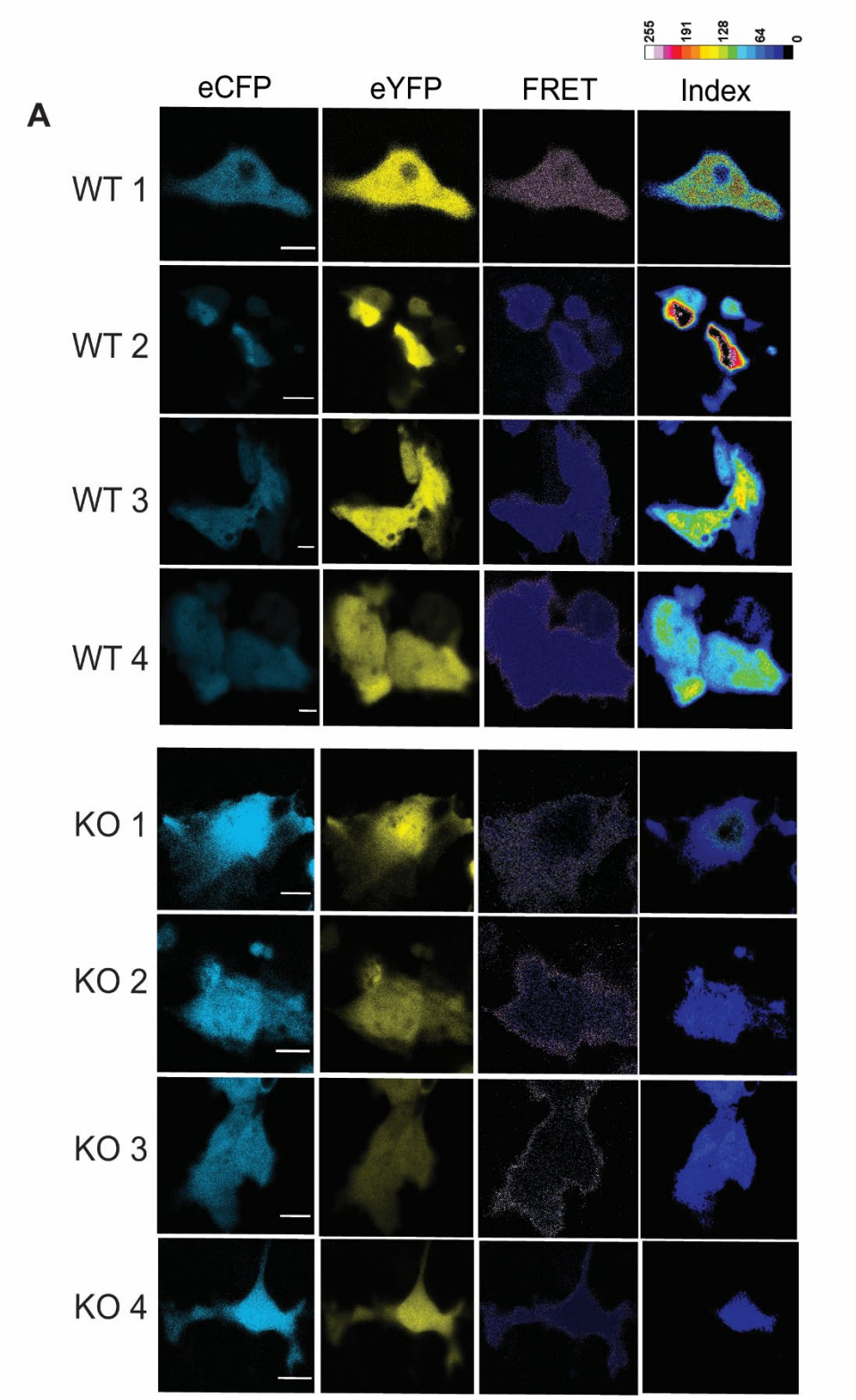

Figure S2. FRET sensor-based visualization of calpain activity in PC cells (Related to Main Fig.2). (A) Representative live cell confocal photomicrographs shows donor (eCFP), acceptor (eYFP) and ratiometric FRET index. High FRET efficiency is detected in WT (WT 1-4) compared to KO PC cells (KO 1-4).

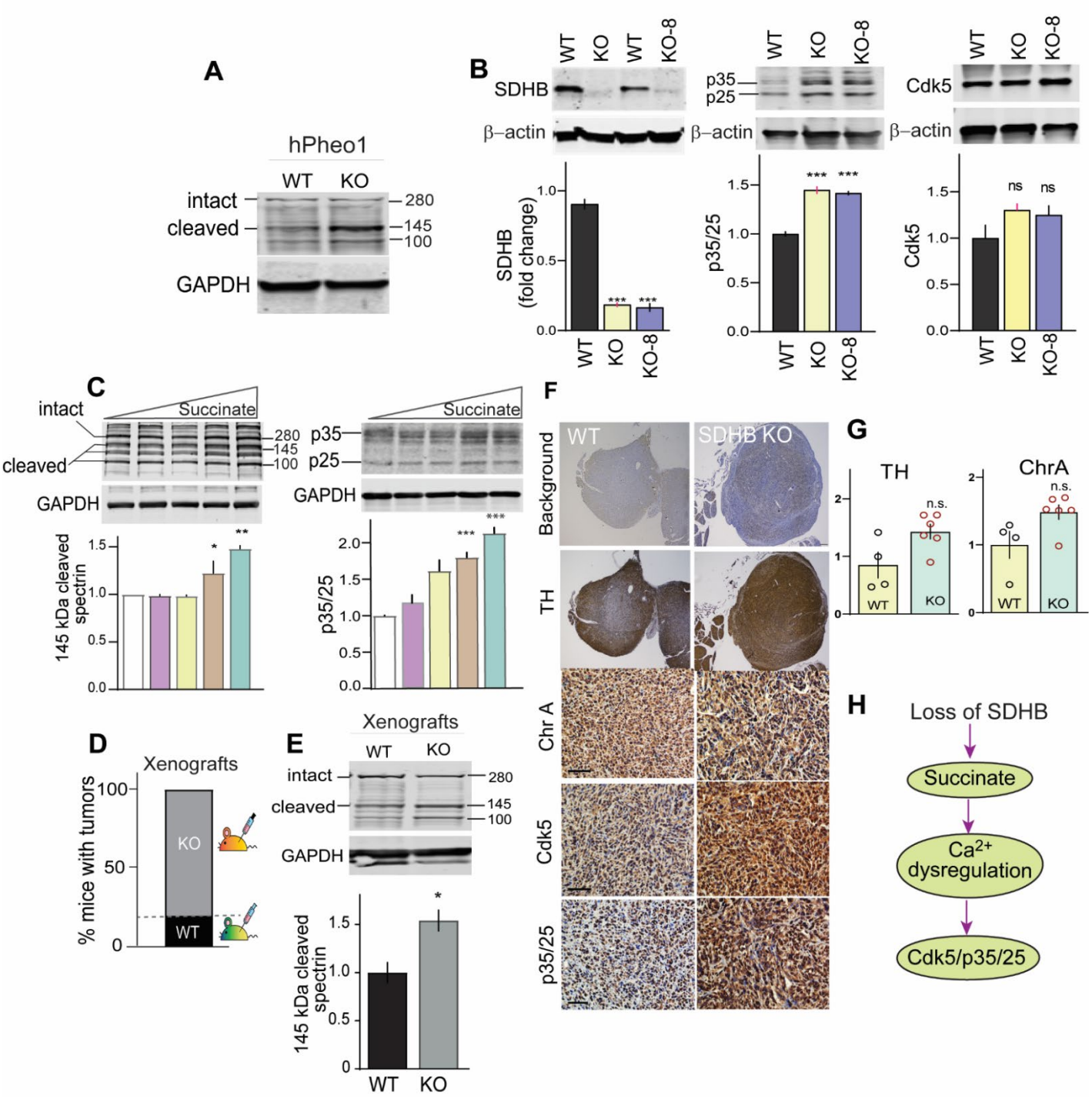

Figure S3. Characterization of *in vitro* and *in vivo* model of hPheo1 (Related to Main Fig.2). (A) Immunoblot showing spectrin cleavage as a function of calpain activity in PC cells. (B) Comparative immunoblot analysis of SDHB, p35/25, and Cdk5 in two independent SDHB KO clones viz. KO vs. KO-8. (C) Quantitative immunoblots showing dose-dependent effect of dimethyl succinate (0, 0.5, 2.5, 5, 10 mM) on spectrin cleavage and p35/25 levels in WT hPheo1. (D) Plot comparing % tumor burden of WT vs. KO hPheo1 derived xenografts. (E) Quantitative immunoblotting of spectrin cleavage in extracts derived from WT (n = 4) and KO (n = 6) xenografts. (F) Immunostains for chromaffin cell neuroendocrine markers, TH, ChrA, Cdk5 and p35/25 in xenograft tissues. (G) Immunoblot quantification of TH, and ChrA in WT and KO tumor tissues as indicated. (H) Signaling schematic showing aberrant Cdk5 as a downstream effector in response to SDHB loss. n = 11 (D) and 4 - 6 (G), values are means ± S.E.M., *p < 0.05, **p < 0.01, ***p < 0.001, n.s. non-significant, Student's *t*-test or one way ANOVA.

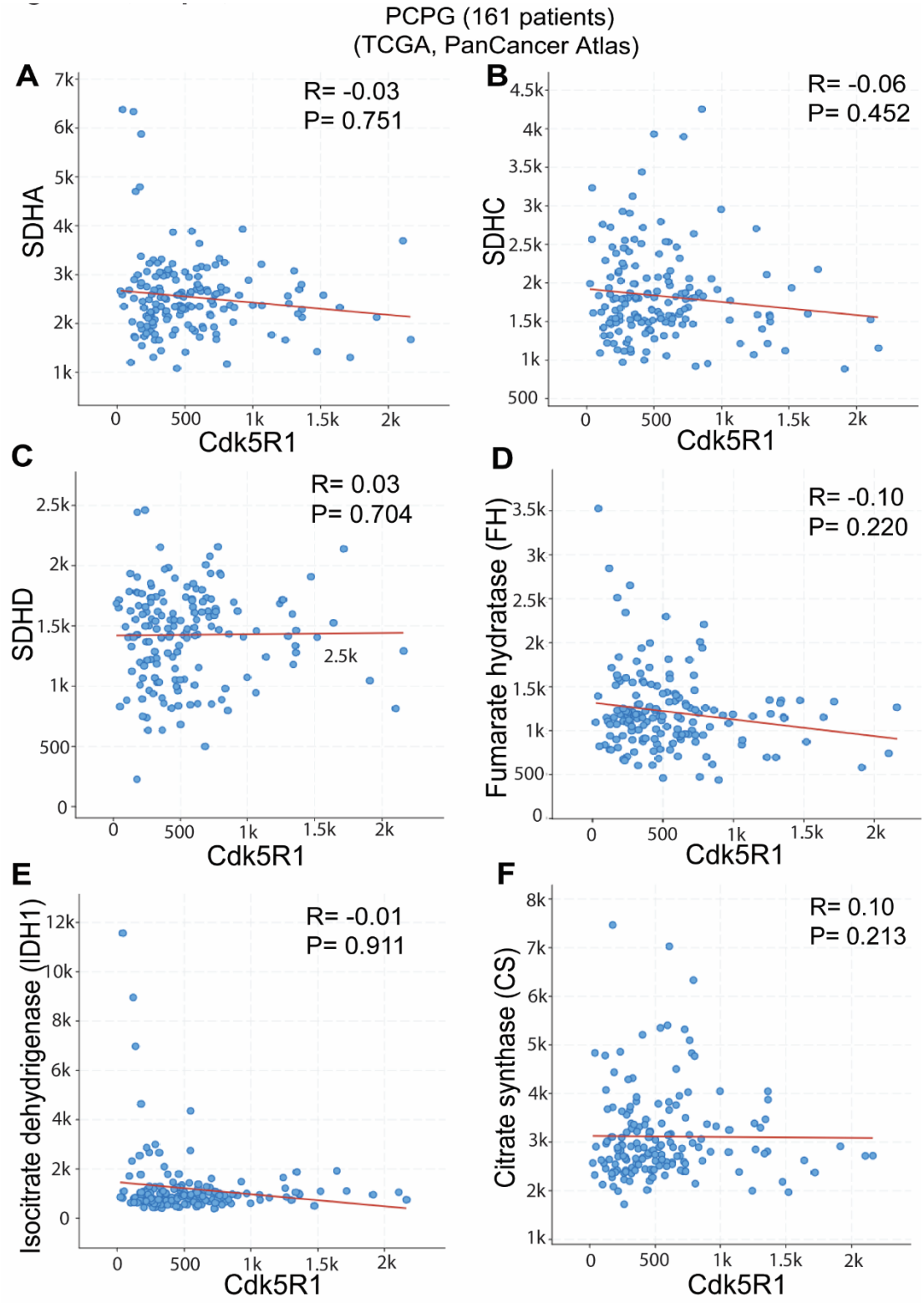

Figure S4. Gene expression correlation analysis for tumor suppressive TCA genes with Cdk5R1 (*i.e* p35) (Related to Main Fig. 3) using cBioPortal. Scatter plot shows Spearman's correlation of Cdk5R1 with (A) SDHA, (B) SDHC, (C) SDHD, (D) FH (Fumarate hydratase), (E) IDH1 (isocitrate hydratase), (F) Citrate synthase (CS).

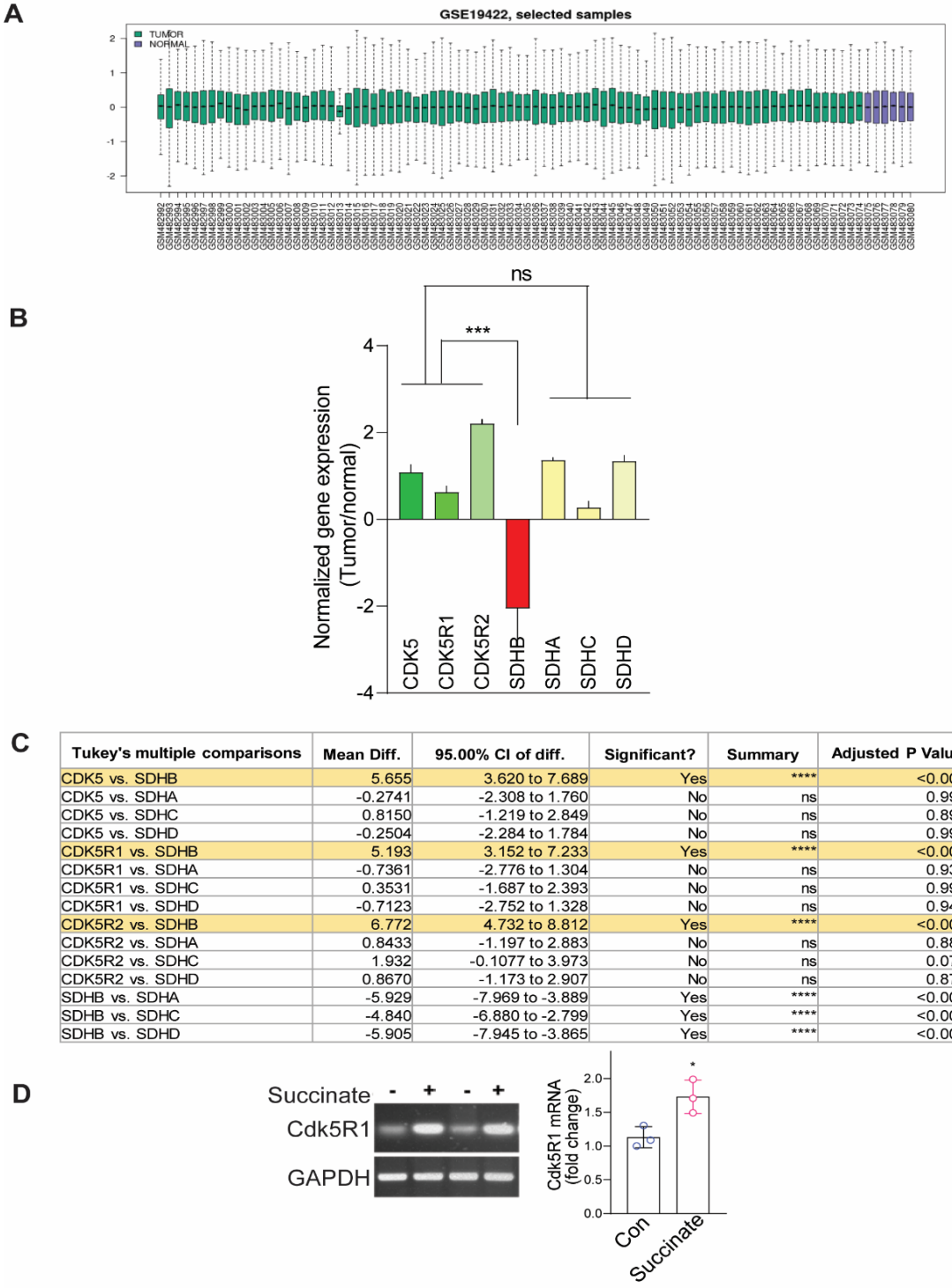

Tukey's multiple comparisons	Mean Diff.	95.00% CI of diff.	Significant?	Summary	Adjusted P Value
CDK5 vs. SDHB	5.655	3.620 to 7.689	Yes	****	<0.0001
CDK5 vs. SDHA	-0.2741	-2.308 to 1.760	No	ns	0.9997
CDK5 vs. SDHC	0.8150	-1.219 to 2.849	No	ns	0.8996
CDK5 vs. SDHD	-0.2504	-2.284 to 1.784	No	ns	0.9998
CDK5R1 vs. SDHB	5.193	3.152 to 7.233	Yes	****	<0.0001
CDK5R1 vs. SDHA	-0.7361	-2.776 to 1.304	No	ns	0.9373
CDK5R1 vs. SDHC	0.3531	-1.687 to 2.393	No	ns	0.9987
CDK5R1 vs. SDHD	-0.7123	-2.752 to 1.328	No	ns	0.9462
CDK5R2 vs. SDHB	6.772	4.732 to 8.812	Yes	****	<0.0001
CDK5R2 vs. SDHA	0.8433	-1.197 to 2.883	No	ns	0.8851
CDK5R2 vs. SDHC	1.932	-0.1077 to 3.973	No	ns	0.0768
CDK5R2 vs. SDHD	0.8670	-1.173 to 2.907	No	ns	0.8709
SDHB vs. SDHA	-5.929	-7.969 to -3.889	Yes	****	<0.0001
SDHB vs. SDHC	-4.840	-6.880 to -2.799	Yes	****	<0.0001
SDHB vs. SDHD	-5.905	-7.945 to -3.865	Yes	****	<0.0001

Figure S5. Gene expression analysis of Cdk5/SDHB signaling components in human PCPG dataset (Related to Main Fig. 3). (A) Box plot showing the distribution of gene expression values for PC (n = 84) and normal adrenal tissues (n = 5) following normalization (NCBI/GEO/GSE-19422). X and Y-axis represent GEO samples and expression values. (B) Plots comparing gene expression values of Cdk5 signaling components with that of SDHB, SDHA, SDHC, and SDHD. (C) Table presents the statistical significance following analysis of gene expression values comparing Cdk5 signaling components with that of SDHB, SDHA, SDHC, or SDHD as indicated; Values are means ± SD ***p < 0.001, n.s. non-significant, Tukey's multiple comparisons test. (D) mRNA expression of Cdk5R1 measured by RT-PCR in wild-type hPheo1 with or without stimulation with succinate (DMS, 10 mM), *p < 0.05.

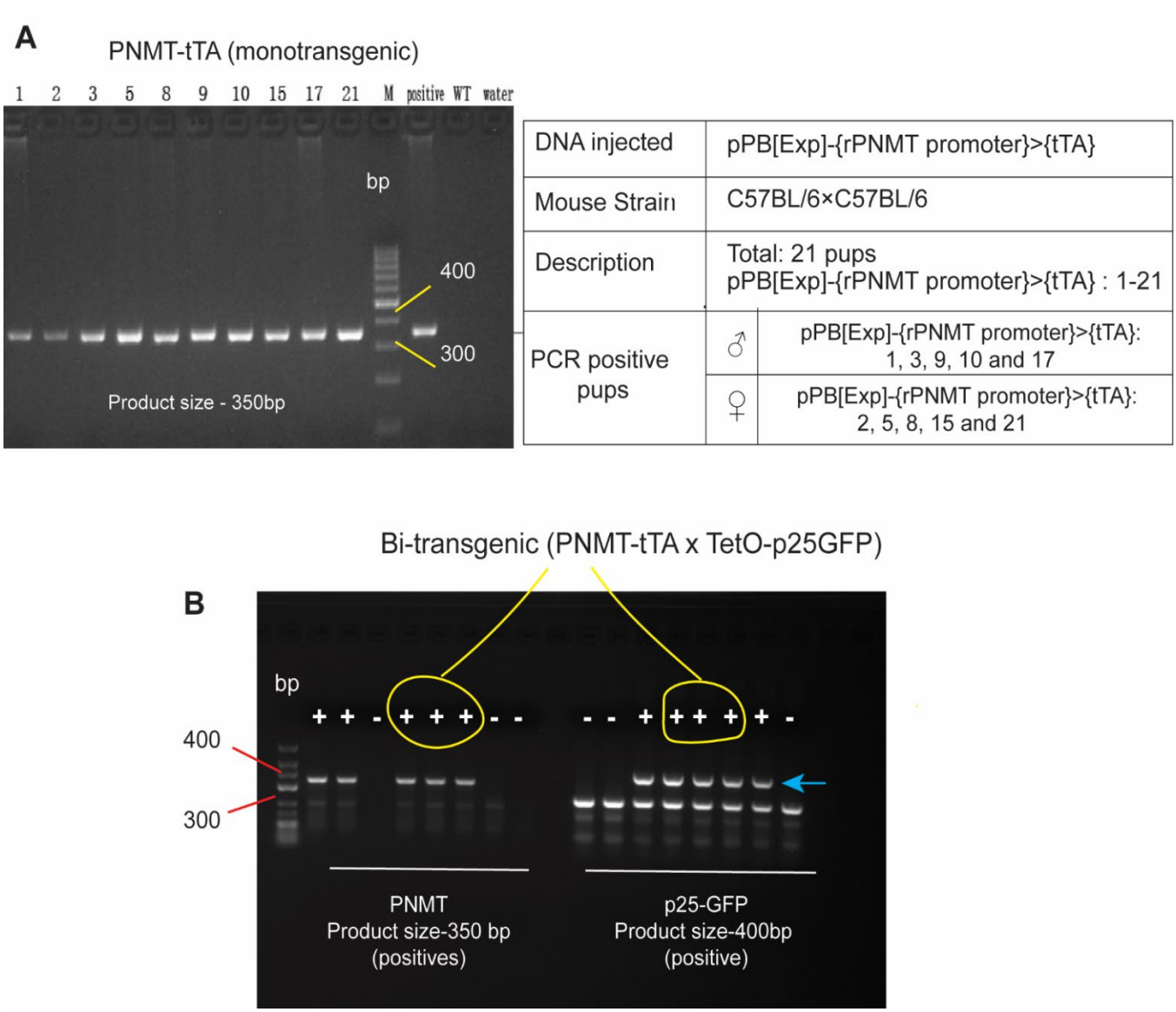

Figure S6. Genotyping of bitransgenic mice (Related to Main Fig. 4). (A) PNMT–tTA littermates were screened to identify positive progeny following PCR analysis using primers described in the methods. Out of 21 pups screened, 10 were positive for PNMT-tTA gene as shown in the table (right). (B) Bi-transgenic pool (PNMT-tTA×TetO-p25GFP) were identified by detecting transgenes expression of PNMT (350 bp) and p25-GFP (400 bp) by RT-PCR.

N	High level GO category	Genes
13	Regulation of response to stimulus	SASH1 TSC1 AAK1 TRIM25 MAPT BCLAF1 GRB7 DEPTOR BAP1 RBL1 CDK12 PRKAG2 POM121
11	Response to stress	SASH1 SEC61B TRIM25 UVRAG BCLAF1 BAP1 TSC1 RBL1 TNKS1BP1 MAPT POM121
11	Regulation of molecular function	SASH1 RBL1 PRKAG2 PKP4 TSC1 UVRAG DEPTOR TBC1D24 MAPT TRIM25 CDK12
10	Regulation of signaling	SASH1 TSC1 AAK1 TRIM25 MAPT GRB7 DEPTOR BCLAF1 CDK12 PRKAG2
9	Catabolic process	SEC61B BAP1 TSC1 MAPT PRKAG2 TRIM25 UVRAG TNKS1BP1 POM121
9	Multi-organism process	TRIM25 YTHDC2 ARID4B CDK13 RBL1 UVRAG DCLK1 SASH1 POM121
8	Macromolecule localization	BAP1 SEC61B POM121 AAK1 DCLK1 TSC1 MAPT PRKAG2
8	Cellular component biogenesis	PKP4 LMOD2 UVRAG RBMX TSC1 MAPT GRB7 BCLAF1
8	Regulation of developmental process	MAPT CDK13 ZC3H13 TSC1 CDK12 RBL1 SASH1 CELSR2
8	Cellular localization	BAP1 SEC61B POM121 DCLK1 TSC1 MAPT UVRAG PRKAG2
8	Regulation of biological quality	AAK1 TSC1 LMOD2 MAPT BAP1 DEPTOR UVRAG TNKS1BP1
7	Anatomical structure morphogenesis	LMOD2 MAPT DCLK1 TSC1 SASH1 CELSR2 GRB7
7	Cell cycle process	RBL1 YTHDC2 PKP4 UVRAG CDK13 PRKAG2 TNKS1BP1
7	Regulation of localization	BAP1 SASH1 AAK1 GRB7 DCLK1 MAPT PRKAG2
7	Regulation of multicellular organismal process	SASH1 MAPT ZC3H13 BAP1 TSC1 CELSR2 TRIM25
6	Immune system process	TRIM25 BAP1 TSC1 CDK13 GRB7 MAPT
6	Response to external stimulus	TRIM25 BAP1 TSC1 DCLK1 SASH1 GRB7
6	Interspecies interaction between organisms	TRIM25 CDK13 RBL1 UVRAG YTHDC2 POM121
5	Growth	MAPT DCLK1 UNC79 CDK11B BAP1
4	Autophagy	TSC1 MAPT UVRAG PRKAG2
4	Cell adhesion	PKP4 TSC1 CELSR2 PLEKHA7
4	Cell proliferation	TSC1 CDK13 BAP1 CDK11B
4	Response to abiotic stimulus	TSC1 TNKS1BP1 MAPT POM121
4	Cell growth	MAPT DCLK1 CDK11B BAP1
4	Biological adhesion	PKP4 TSC1 CELSR2 PLEKHA7
4	Locomotion	SASH1 GRB7 TRIM25 DCLK1
4	Regulation of cellular component biogenesis	TSC1 LMOD2 MAPT BCLAF1
3	Immune effector process	TRIM25 TSC1 CDK13
3	Immune response	TRIM25 TSC1 CDK13
3	Behavior	UNC79 TSC1 MAPT
3	Response to biotic stimulus	TRIM25 DCLK1 SASH1
3	Regulation of cell adhesion	TSC1 CELSR2 PKP4
3	Regulation of growth	MAPT CDK11B BAP1
3	Regulation of locomotion	SASH1 GRB7 TRIM25
3	Regulation of multi-organism process	TRIM25 YTHDC2 SASH1
3	Leukocyte activation	TSC1 CDK13 MAPT
3	Developmental growth	MAPT DCLK1 UNC79
3	Anatomical structure formation involved in morphogenesis	LMOD2 TSC1 SASH1
3	Cell motility	SASH1 GRB7 DCLK1
3	Localization of cell	SASH1 GRB7 DCLK1
3	Response to other organism	TRIM25 DCLK1 SASH1
2	Reproduction	YTHDC2 ARID4B
2	Immune system development	TSC1 CDK13
2	Developmental process involved in reproduction	YTHDC2 ARID4B
2	System process	LMOD2 MAPT
2	Response to endogenous stimulus	TSC1 MAPT
2	Sexual reproduction	YTHDC2 ARID4B
2	Reproductive process	YTHDC2 ARID4B
2	Methylation	ARID4B ZC3H13
2	Multicellular organism reproduction	YTHDC2 ARID4B
2	Multi-organism reproductive process	YTHDC2 ARID4B
2	Multicellular organismal reproductive process	YTHDC2 ARID4B

Figure S7. **Table showing enriched GO category (biological processes) corresponding to the downregulated Cdk5 targets in p25OE tumors** (data derived from ShinyGO, followed by FDR correction; p-value cutoff = 0.05) (Related to Main Fig. 5).

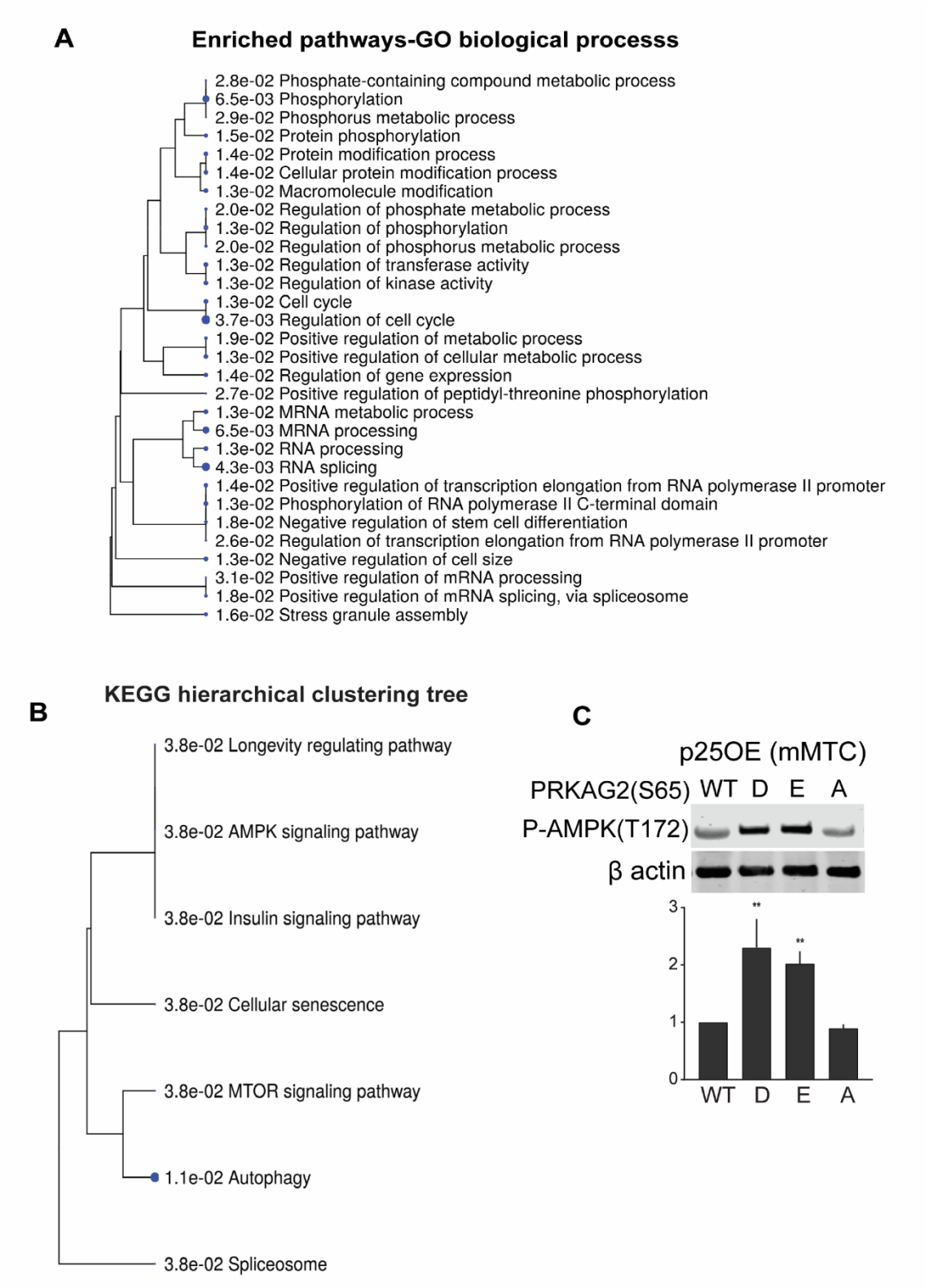

Figure S8. **Relation among enriched GO molecular pathways** visualized as (Related to Main Fig. 5) (A) Hierarchical clustering tree, and (B) Kyoto Encyclopedia of Genes and Genomes (KEGG) pathway analysis. Downregulated phospho-target genes mostly involved in cellular metabolic and protein phosphorylation processes as shown. (C) Quantitative immunoblotting of (P-T172) AMPK catalytic phosphorylation in response to PRKAG2 S65D/E/A phosphosite mutant expression in p25OE mMTC cells (mouse Medullary Thyroid Carcinoma cells). Values are means ± SEM, **$p < 0.01$, $n = 3$.

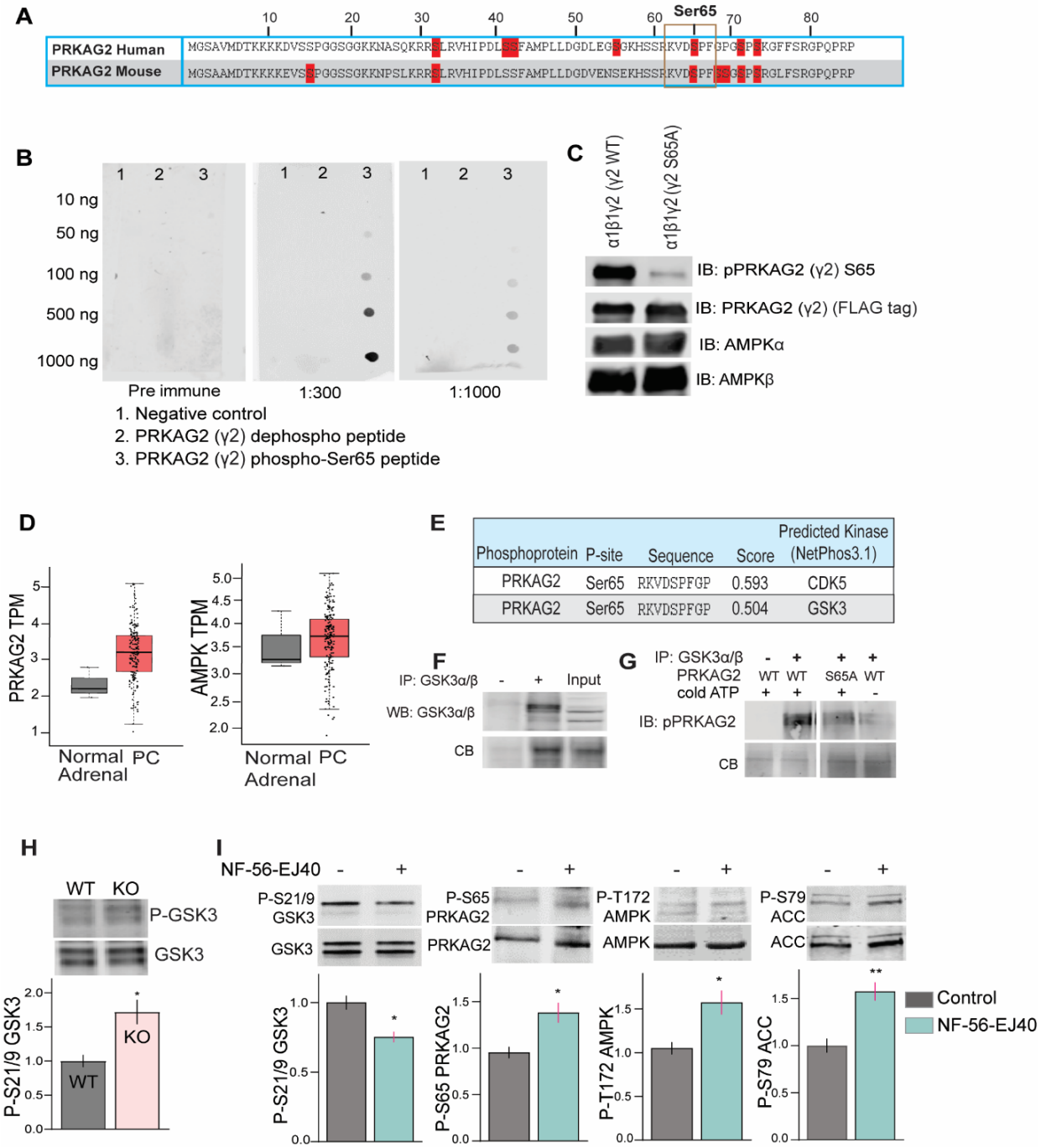

Figure S9. Generation of phospho-Ser65 PRKAG2 antibody (Related to Main Fig. 5 and 6). (A) Clustal omega alignment shows conservation of Ser65 in human and mouse PRKAG2 amino acid sequence. (B) Dot blots shows selective reactivity of anti-serum for P-PRKAG2 peptide. (C) AMPK holo-complex (α1β1γ2) comprised of WT or S65A PRKAG2 phosphorylated by GSK3β *in vitro,* demonstrating the specificity of affinity purified antibody. (D) The mRNA expression of PRKAG2 and AMPKα in PC vs. Normal Adrenals; Gene Expression Profiling Interactive Analysis; p-value cutoff 0.05. (E) NetPhos3.1 prediction of upstream kinases that phosphorylates Ser65 PRKAG2. (F-G) IP kinase assay performed to phosphorylate purified PRKAG2 (WT, S65A) incubated with immunoprecipitated GSK3 (F) in the presence of cold ATP at 30°C for 60 min. The reaction products were probed with P-Ser65 PRKAG2 antibody (G), CB = Coomassie blue stained protein. (H). Immunoblots densitometry shows differential expression levels of P-GSK3 in WT vs. *SDHB* KO cells. (I) Immunoblots quantitation showing expression of P-GSK3, P-PRKAG2, P-AMPK, P-ACC in KO hPheo1 upon treatment with NF-56-EJ40.

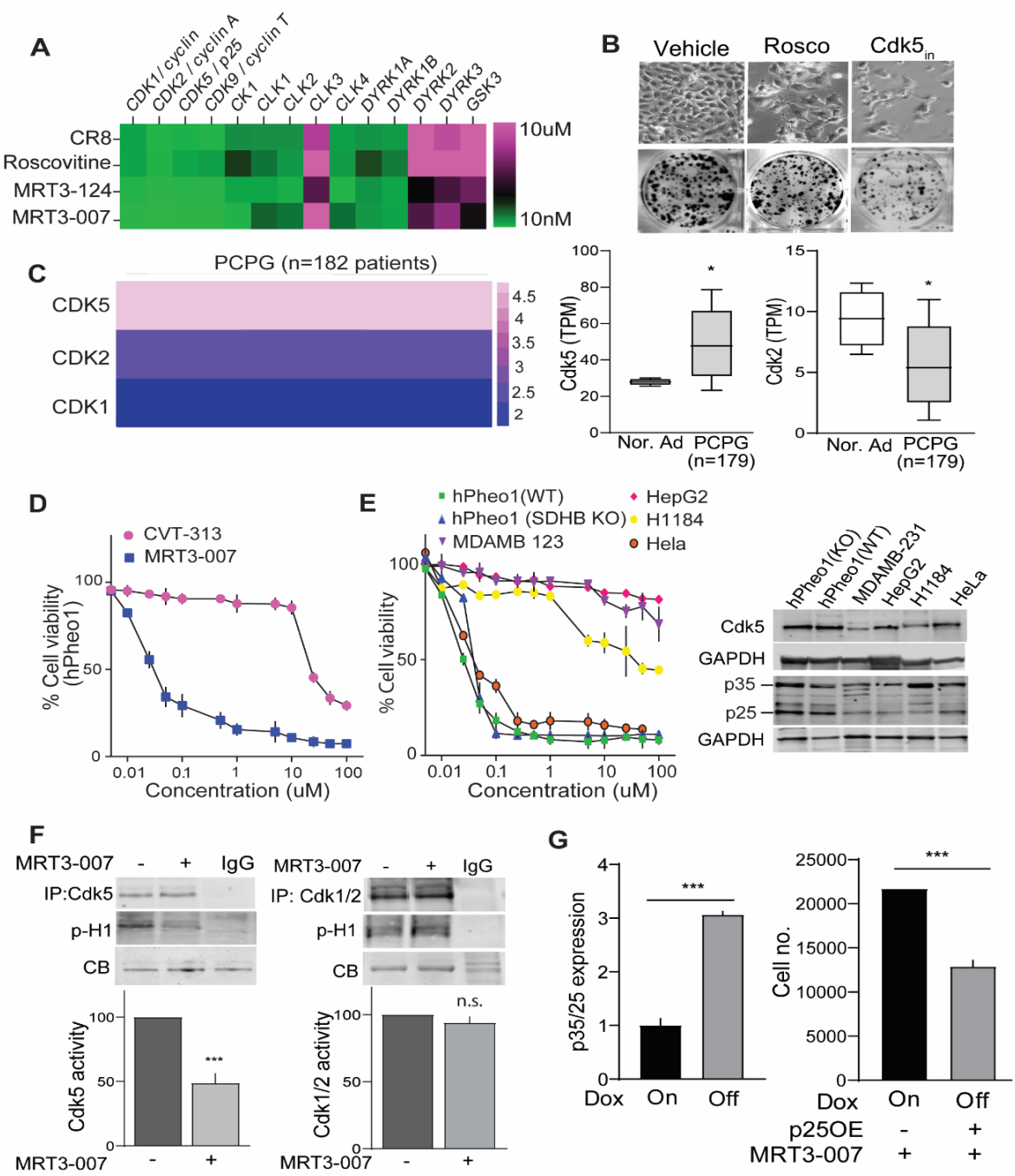

Figure S10. Selectivity assessment of MRT3-007 (Cdk5$_{in}$) (Related to Main Fig. 6). (A) IC_{50} heatmap showing *in vitro* kinase profile of Cdk5 inhibitors. (B) Effects of Cdk5 inhibitors on cell morphology and colony formation. (C) Heatmap shows gene expression of Cdk5, Cdk2, and Cdk1 in human PCPG (left). Bar graphs compare Cdk5/Cdk2 transcript levels in normal adrenals vs. PC (right). (D) Growth inhibitory effects of Cdk5$_{in}$ compared to that of the Cdk2 inhibitor (CVT-313) on hPheo1. (E) Dose-dependent effect of MRT3-007 on different cancer cell types (left) expressing high and low levels of Cdk5/p35/25 as indicated by immunoblot in right. Note: MRT3-007 was least effective in cells expressing the lowest levels of p25 (MDAMB-231, HepG2, and H184). Values are means ± S.E.M., n = 3. (F) IP kinase assays with immunoblot for histone H1 phosphorylation (p-H1) with Cdk5 (left) and Cdk2 (right) immunoprecipitated from hPheo1 cell lysates treated with vehicle (-) vs. MRT3-007 (+) for 12 h. Coomassie blue (CB) staining shows total histone H1 protein levels. (G) Immunoblot quantitation confirming elevation of p25 in Dox OFF cells (left) as shown with the effect of MRT3-007 on cell viability of p25-ON vs. p25-OFF NE cells (right). Data are means ± S.E.M., ***$p < 0.001$, n.s. non-significant; Student's *t*-test, n = 3.

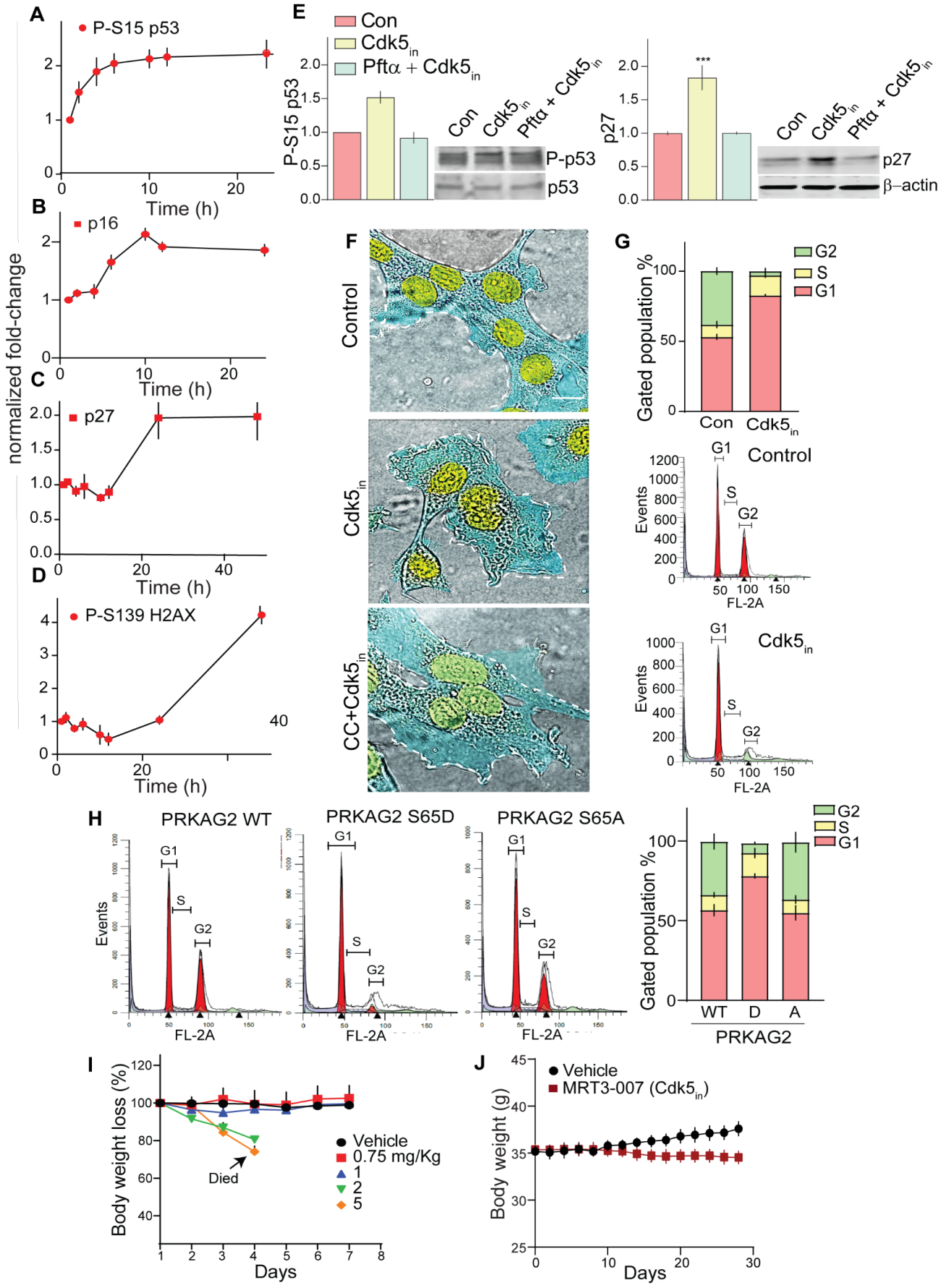

Figure S11. Inhibition of p53 or AMPK abrogate effects of Cdk5$_{in}$ (Related to Main Fig. 7). Immunoblots quantification showing time-dependent effect of Cdk5$_{in}$ on phosphorylation states of (A) P-S15 p53, (B) p16^{INK4a},(C) p27^{Kip}, (D) P-S139 H2AX. Values

presented as fold change normalized with time = 0, n = 3, Values are means ± S.E.M. (E) Immunoblot densitometry detects P-p53 and $p27^{Kip}$ upon $Cdk5_{in}$ treatment in the presence or absence of p53 inhibitor PFT-α (10 μM, 10 h pre-treatment). (F) Phase contrast microphotographs showing effects of AMPK inhibitor, Compound C (CC, 10 μM) on $Cdk5_{in}$ induced morphological changes. (G) Representative DNA histogram showing cell cycle profile of KO cells treated with vehicle or $Cdk5_{in}$ (20 nM); histograms analysis by MODfit LT 3.0 presents cell cycle distribution in G1 (orange), early-S (yellow), and late-S/G2/M (green); n = 2, Values are means ± SD. (H) Representative histograms and quantitation indicate cell cycle profile of KO hPheo1 expressing either WT, S65D or S65A phosphomutants of PRKAG2. (I) Maximum tolerated dose (MTD) of $Cdk5_{in}$ [MRT3-007] in C57BL6 mice expressed as body weight (% of original). Mice were injected with escalating doses of 0.75, 1, 2, or 5 mg/kg MRT3-007, respectively (n = 5). (J) Time-dependent effect of vehicle or MRT3-007 (0.5 mg/kg) on body weight of SDHB KO xenografts (n = 4).

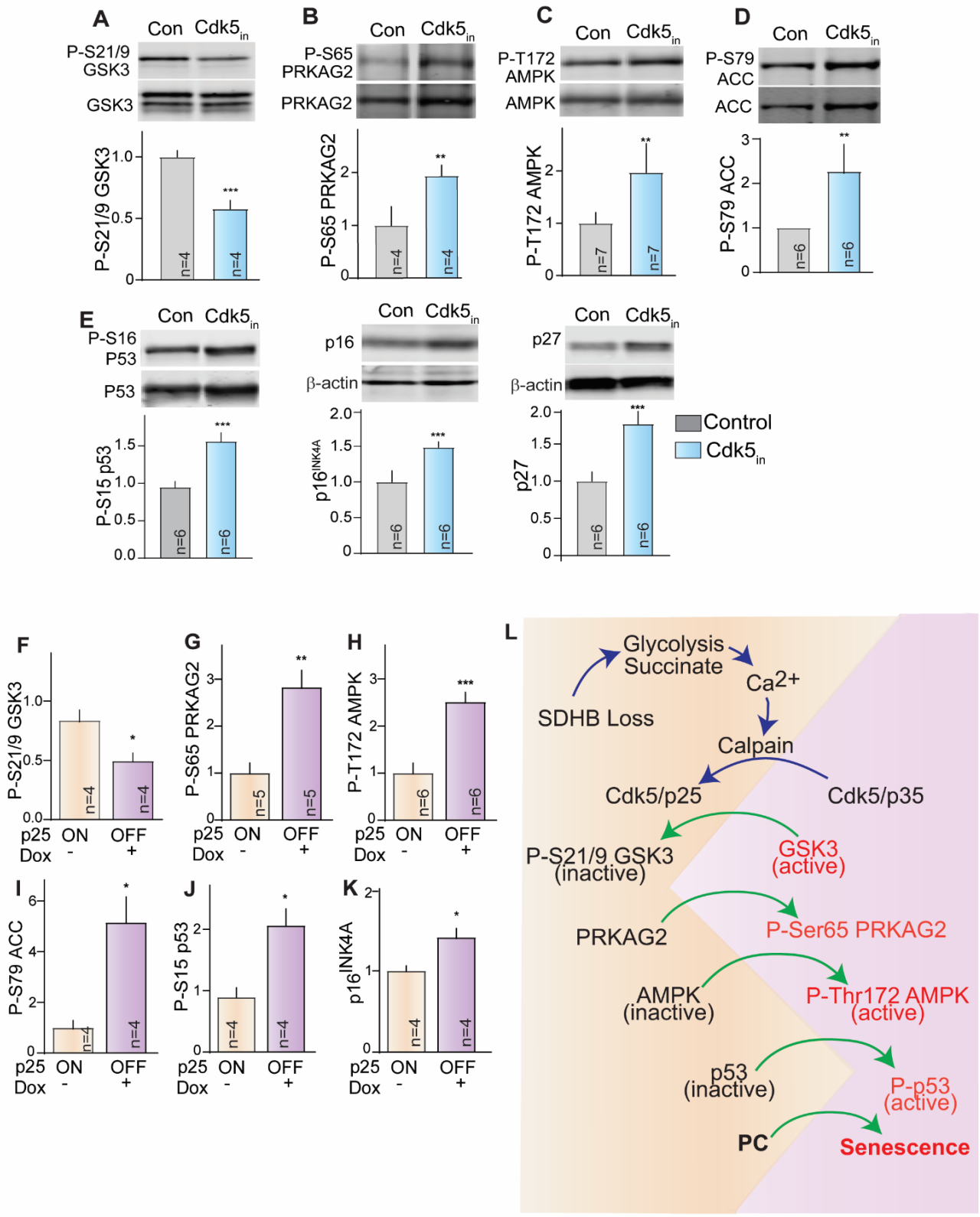

Figure S12. Cdk5 inhibition attenuates *in vivo* tumor growth (Related to Main Fig. 7). (A-E) Quantitative immunoblots of phosphorylation sites and proteins in *SDHB* KO xenograft tumor lysates as shown. (F-K) Immunoblot quantitation of indicated phosphorylation site or protein from p25ON/OFF tumors derived from bitransgenic mice. Data are means ± SEM; *p < 0.05, ** p < 0.01, ***p < 0.001, Student's *t*-test. (L) Schematic depicting the signaling cascade delineated in these studies downstream of SDHB loss.